The Development of an Indexing Method for the Comparison of Unbalanced Magnetic Pull in Electrical Machines

The Measurement and Indexing of Unbalanced Magnetic Pull in Electrical Machines

Introduction

Unbalanced magnetic pull (UMP - a radial decentering force on the rotor, caused by rotor non-centering and other asymmetries) is hard to measure. In addition, it has been studied in several machines but there is also a lack of some sort of indexing to enable relative comparison of the UMP characteristics between different motors and different sizes.

Unbalanced magnetic pull is important because it affects the wear on the bearings [1] as well as noise and vibration [2]. This is particularly the case in brushless servo motors where fractional slots are used [3]. However, the most common form of UMP is due to the rotor not being centered in the stator bore. There are two types of rotor center displacement, or as it is termed, eccentricity: static eccentricity where the rotor is not centered in the stator bore but still turning on its own axis; and dynamic eccentricity where the rotor is not turning on its own axis but is turning on the stator axis. Obviously both can exist simultaneously and many condition monitoring methods which use the monitoring of current sideband components in induction motors rely on this [4][5]. The sources of static eccentricity could be a worn or displaced rotor bearing while a bent shaft, mechanical unbalance in the rotor, or rotor resonance [6] can cause dynamic eccentricity. Most research studies assume that the rotor eccentricity is uniform although a bent shaft or misplaced bearing will mean the eccentricity varies down the axial length. There have been some models that take this into account [7].

The papers [1] to [7] describe UMP in induction motors except for [3], which considers UMP in a permanent magnet machine. UMP is an important issue in any electrical machine and examples of UMP in other machines are given in [8]-[12]. However, because the induction machine has a secondary circuit, where the rotor current requires calculating, UMP in induction motors is more complicated to calculate compared to other electrical machines. However, many machines will be competing for use in different applications. For instance, wind turbine generators can be wound or cage rotor induction generators, permanent magnet generators and wound field synchronous generators. Automotive drive motors are mostly using interior permanent magnet motors but induction motors are increasingly being used. Being able to quantify the characteristic UMP will be helpful in terms of being aware of the required mechanical stiffness, allowable tolerance of bearing wear, and manufacturing tolerances. It has to be remembered that UMP will vary with voltage and load. This is one of the focuses of this digest and the full paper will further elaborate on this. The machines covered are induction, permanent magnet and synchronous machines that all tend to have 3 phase distributed windings and cylindrical stators. Switched reluctance machines also exhibit UMP although rotating field theory is difficult to implement in this machine. The effects of UMP for this sort of machine were addressed in [13].

Core saturation and windings can affect the UMP. For the induction motor, at a set speed, the UMP should go up with the square of the voltage but as illustrated in [14] saturation attenuates the UMP. Parallel stator windings and the rotor cage can also reduce UMP (and create additional vibration)[15] whereas skew increases the UMP [16]. In the permanent magnet motor the rotor topology has a great effect [17] and also parallel windings can have an effect [18].

As already stated, measuring UMP is difficult. In machines with magnetic bearings [19] or bearingless machines [20] the force can be calculated using the currents in the levitation system. Load cells have been used [21] although they do move when loaded which needs to be taken into account. A more successful mechanical method is to use piezoelectric force cells. These were used in [15][22][23] in the form of a load table or plate. The stator was mounted on the table and the rotor separately mounted on pedestals. The rotor and stator can then be moved with respect to each other and the UMP assessed. The transducers have negligible movement. A development of this method is to put the transducers in the rotor pedestals. This method is reported in this digest.

This digest reports on experimental methods that have been developed to measure UMP and an indexing technique to allow direct comparison of UMP between different machines. It will develop the indexing method and use machines tested on the developed experimental rigs, and in other studies, to calculate and compare the soundness of the index. The index method is primarily aimed at cylindrical AC machines with rotation flux waves.

UMP Index

UMP is due to an imbalance in the air-gap magnetic flux. As described in many studies, if the rotor is not centred then permeance modulation of the MMF takes place so that for a p pole-pair machine, there will not only be a p pole-pair magnetic flux wave but also $p\pm1$ pole-pair magnetic flux waves. Indeed, at a high degree of rotor eccentricity then there will be even more flux waves ($p \pm 2$, 3, etc) [24]. However, at low eccentricity it is the $p\pm1$ poles that are most prevalent and this is what we will focus on. Let us assume that we have a rotating MMF source. This could be a distributed winding or indeed a magnet source. If it is assumed to be sinusoidal then

$$j_{MMF}^{p}(y,t) = J^{p}\cos\left(\omega t - pky + \phi_{p}\right) = \mathrm{Re}\left\{\bar{J}^{p}e^{j(\omega t - pky)}\right\} \quad (1)$$

where y is the circumferential distance around the airgap, ω is the angular velocity of the supply, p is the pole-pair of the MMF wave, and k is the inverse of the average airgap radius r. If the rotor is not centered and the eccentricity is uniform down the axial length, then an approximate airgap length when the rotor has either static or dynamic eccentricity is

$$g_s(y) = g\left(1-\delta_s\cos(ky)\right) \text{ and } g_d(y,t) = g\left(1-\delta_d\cos(\omega_r t - ky)\right) \tag{2}$$

To get the permeance wave then the gap length expressions can be inverted

$$\Lambda_s(y) = \frac{1}{g}\left(1+\delta_s\cos(ky)\right) \text{ and } \Lambda_d(y,t) = \frac{1}{g}\left(1+\delta_d\cos(\omega_r t - ky)\right) \tag{3}$$

The amount of eccentricity $\delta_{s,d} = x/g$ where x is the actual rotor displacement and g is the air-gap length when the rotor is centred. The rotor rotational velocity is ω_r. This gives the airgap flux density waves as

$$b(y,t) = \mathrm{Re}\left\{\bar{B}^p e^{j(\omega t - pky)} + \bar{B}_\delta^{p-1} e^{j(\omega_A t - k(p-1)y)} + \bar{B}_\delta^{p+1} e^{j(\omega_B t - k(p+1)y)}\right\}\Big|_{\substack{\text{Low slip}\\ \text{Low eccentricity}\\ \text{Space harmonics neglected}}} \tag{4}$$

where, for static eccentricity $\omega_A = \omega_B = \omega$ and for dynamic eccentricity $\omega_A = \omega - \omega_r$ and $\omega_B = \omega + \omega_r$.
The field magnitude coefficients (which are phasors) are

$$\bar{B}^p = \frac{j\mu_0\bar{J}}{kpg} \text{ and } \bar{B}_\delta^{p\pm1} = \frac{j\mu_0\bar{J}}{kpg}\delta_{s,d} = \bar{B}^p\delta_{s,d} \tag{5}$$

We can address the normal Maxwell stress σ at any point in the airgap. This is the primary sources of UMP:

$$\sigma(y,t) = \frac{B_r^2 - B_t^2}{2\mu_0} \approx \frac{B_r^2}{2\mu_0} = \frac{\left|b(y,\mathrm{t})\right|^2}{2\mu_0} \tag{6}$$

where B_r is the flux density in the radial direction and B_t is the flux density in the tangential direction in the airgap at a circumferential distance y. For a machine with axial length L and mean airgap radius r, the force in the α direction (α and β being Cartesian coordinates for a cross-section and the eccentricity and force being in the α direction):

$$F_\alpha = L\int_0^{2\pi r}\frac{\sigma(y,t)}{2\mu_0}\cos(ky)\,dy = L\int_0^{2\pi r}\frac{\left|b(y,t)\right|^2}{4\mu_0}\left(e^{jky}+e^{-jky}\right)dy \tag{7}$$

Focussing on static eccentricity for simplicity, this will create a constant side force. Dynamic eccentricity will develop a rotating force vector. The airgap flux density waves can be written as

$$b(y,t) = \mathrm{Re}\left\{\bar{B}^p\left(e^{j(\omega t - pky)} + \delta_s\left(e^{j(\omega t - k(p-1)y)} + e^{j(\omega t - k(p+1)y)}\right)\right)\right\} \tag{8}$$

For the force in (7) the square of magnitude is required. However, only 2-pole waves are needed in (7) for non-zero solving:

$$\left|b(y,t)\right|^2_{\text{2 pole waves only}} = \left(\mathrm{Re}\left\{\frac{\delta_s\left|\bar{B}^p\right|^2 e^{jky} + \delta_s\left|\bar{B}^p\right|^2 e^{-jky}}{2}\right\}\right) \tag{9}$$

The 2-pole force waves are generated by flux waves with pole numbers differing by two. This generates UMP [7]. Hence

$$F_\alpha = L\int_0^{2\pi r}\frac{\left|b(y,t)\right|^2_{\text{2 pole waves only}}}{4\mu_0}(e^{jky}+e^{-jky})\,dy = \frac{L}{8\mu_0}\delta_s\left|\bar{B}^p\right|^2\int_0^{2\pi r}\mathrm{Re}\left\{(e^{jky}+e^{-jky})(e^{jky}+e^{-jky})\right\}dy = \frac{\pi Lr}{2\mu_0}\delta_s\left|\bar{B}^p\right|^2 \tag{10}$$

The UMP flux coefficient can then be assessed where $C_{UMP}^{Flux} = \dfrac{2\mu_0 F_x^{\text{measured}}}{\pi Lr\delta_s\left|\bar{B}^p\right|^2}$ (11)

It is more useful to have a coefficient that is a function on an easy measureable component such as the terminal voltage or back-emf. The voltage induced into one phase is

$$\begin{aligned} u_{phase}(t) &= \mathrm{Re}\left\{-2\pi rL\frac{\omega\bar{B}^p}{kp}\bar{N}^{*p}_{phase}e^{j\omega t}\right\} = \mathrm{Re}\left\{-2\pi rL\frac{\omega\bar{B}^p}{kp}e^{j\omega t}\frac{1}{2\pi r}\sum_{w=1}^{W}C^w_{phase}e^{-j\theta_w}\right\} \\ &= \mathrm{Re}\left\{-\frac{rL\omega\bar{B}^p}{p}e^{j\omega t}\sum_{w=1}^{W}C^w_{phase}e^{-jky_w}\right\} \approx \mathrm{Re}\left\{-\frac{2rL\omega\bar{B}^p}{p}N_{phase}e^{j\omega t}\right\}\Big|_{\substack{\text{Winding factor}\\ \text{close to unity and}\\ \text{centered on the y axis}}} \end{aligned} \tag{12}$$

which means the force can be denoted in terms of the voltage:

$$\left|F_x\right| = \frac{\pi Lr}{2\mu_0}\delta_s\left|\bar{B}^p\right|^2 = \frac{\pi Lr}{2\mu_0}\delta_s\frac{p^2\hat{V}^2_{phase}}{\left(2rL\omega N_{phase}\right)^2} = \frac{\pi p^2\delta_s V^2_{phase-rms}}{4\mu_0 rL\omega^2 N^2_{phase}} \tag{13}$$

This has many simplifications and does not take into account winding harmonics and saturation. It assumes sinusoidal phase voltage. However we can now write an expression for the UMP voltage coefficient so that

$$C_{UMP}^{Voltage} = \frac{4\mu_0 rL\omega^2 N^2_{phase}\left|F_x\right|}{\pi p^2\delta_s V^2_{phase-rms}} \tag{14}$$

The voltage coefficient increases with increasing UMP and decreasing voltage. To get an index where a high value represents low relative UMP, we can use

$$\text{UMP factor} = {}^{1}\!\Big/\!_{C_{UMP}^{Voltage}} \tag{15}$$

The eccentricity is a function of the relative eccentricity. Therefore for a given UMP factor then a larger airgap is more advantageous because the rotor has to be displaced further in actual terms to produce the same amount of UMP. We can normalize the airgap in an arbitrary manner where an airgap of 0.5 mm =1 so that

$$\text{UMP-gap factor} = {}^{2g[\text{mm}]}\!\Big/\!_{C_{UMP}^{Voltage}} \tag{16}$$

The UMP and UMP-gap factors can be below or above 1 depending on whether there is damping of the additional flux waves generated by the eccentricity, say by a rotor cage, or whether the machine airgap is flux-wave rich. The results section presents a survey of different machines in order to validate these factors.

Measurement

Few studies have measured UMP. In bearingless machines, it can be related to the control currents [26] and complex strain gauge methods were discussed in [18]. A good method is to use piezoelectric transducers. They can be used in a mounting plate with the stator mounted on the plate and the rotor separately mounted on pedestals. This was done in [15]. A more versatile method is to incorporate transducers into the rotor support pedestals and this has now been done as illustrated in Fig. 1. Two rigs are illustrated: these have been developed independently but use similar arrangements. To focus on the rig in Figs. 1(a) and (b), the rotor mountings were shimmed to try to get the rotor and stator at the same height and the stator adjusted in the x direction as indicated. The center rotor position was set using feeler gauges in the airgap at the ends of the rotor. This illustrated that setting the rotor location is not straightforward. Fig. 1(c) shows another rig which is single sided (just two on one rotor mounting). For the first rig, the stator was moved using simple clock gauges. The voltage was varied at different eccentricity values to get a set of characteristics. Since it is a wound rotor machine the rotor could be open circuit and short circuit.

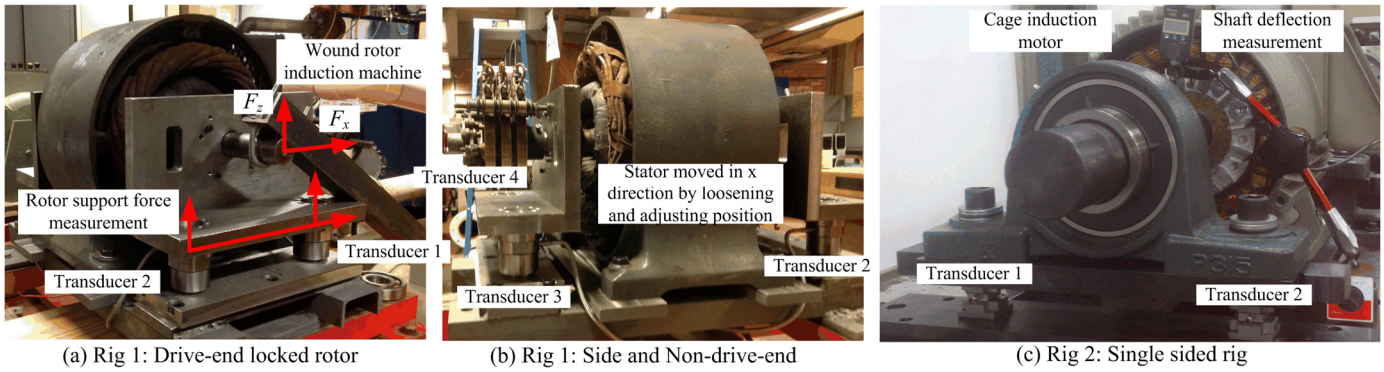

(a) Rig 1: Drive-end locked rotor (b) Rig 1: Side and Non-drive-end (c) Rig 2: Single sided rig

Fig. 1. UMP Measurement rigs using Piezo-electric force transducers.

The torque and force can be measured using these rigs if they are not connected to a load. If the rotor is locked then torque can be separated out from the UMP by measurement of forces when the rotor locking bar is against the rotor support (no torque detected) then supported against the motor bed (torque and UMP both detected). For the UMP, and using the coordinate system in Fig. 2:

$$Fz_{Total} = Fz_1 + Fz_2 + Fz_3 + Fz_4 \quad \text{and}$$
$$Fx_{Total} = Fx_1 + Fx_2 = {}^{x}\!\Big/\!_{y}\left(Fz_1 - Fz_2 - Fz_3 + Fz_4\right) \tag{17}$$

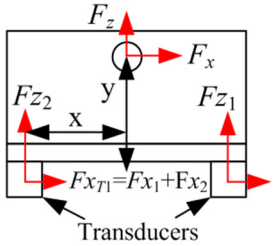

Four transducers, for x and z directions there are three channels per rotor end: Fz_1, Fz_2, Fx_{T1} for drive end, Fz_3, Fz_4, Fx_{T2} for NDE

Fig. 2. Drive-end force coordinates.

If the rotor mounting geometry is given in Fig. 2, where the angle θ is defined by $\tan(\theta) = {}^{x}\!\Big/\!_{y}$, the torque, when the locking bar is against the rig bedplate, is

$$\text{Torque} = \left[\left(Fz_1 - Fz_2\right)\cos(\theta) + Fx_1\sin(\theta) + \left(Fz_4 - Fz_3\right)\cos(\theta) + Fx_2\sin(\theta)\right] \tag{18}$$

This is in addition to the UMP. The full paper will give a full set of results although in this digest only some selected results are given for validation of the UMP and UMP-gap factors.

Results

The full paper will give a wide survey of UMP in different machines and put forward experimental results from different machines tested on the rigs described above. Table I shows a survey of different machines in tabular form. The different

geometries are put forward and, using the measured or calculated UMP, the UMP and UMP-gap factors are calculated. As already stated, high factor means low relative UMP.

The survey includes a 10 pole induction machine from previous studies which had either a blank laminated cylindrical rotor with a large airgap (1.5 mm), or a cage rotor with a 0.5 mm airgap. For the blank rotor, when the 3-phase windings are in series, show a UMP factor close to unity. The UMP-gap factor is higher because the airgap is relatively large. When the winding contains parallel paths, which are known to damp UMP, the factors increase. For the cage rotor, at no load, dynamic eccentricity has a UMP factor close to unity again but the static eccentricity gives a high UMP factor. It was explained in [7] that the cage rotor will damp the UMP but not in the no-load dynamic eccentricity case. At locked rotor the factors are very low because the damping of the UMP by the rotor decreases as the effects of the differential and slotting increase [7]. A 4 pole wound rotor machine was tested in the rig in Fig 1 (a) and (b) and it can be seen that the UMP factor under no load is 0.72 but decreases under locked rotor conditions with the rotor shorted for the same reasons as described above. The 4 pole machine tested in [5] and [7] again confirms the lack of UMP damping with dynamic eccentricity at no load with a UMP factor of 0.8. A 6 pole machine was tested in the rig in Fig. 1(c) using a DC test so that there was no rotor current and as expected the UMP factor was almost unity.

Further machines assessed were brushless permanent machine machines. Additional types of this machine will be tested and reported. The simulation of a rare-earth magnet machine in [25] gave good UMP factors and these results were echoed by the 12 pole surface magnet machine in [17]. These were under no load conditions however the UMP factor reduced when the 12 pole machine was loaded. This will be due to additional MMF harmonics since it is a fractional slot machine and additional vibrations were produced. The consequent magnet rotor designs (where the poles alternate between surface magnets and steel poles so there is one magnet per pole-pair) in [17] and [25] have reduced UMP factors compared to the surface magnet machines, i.e., they generate more UMP. This has been reported in [15] as a major characteristic of the consequent rotor machine, hence its use as a bearingless machine. The full paper will include an internal permanent magnet machine and a synchronous machine, as well as larger machines, for completeness.

The UMP-gap factors are higher when the airgap is larger and this reflects the fact that a bearing can wear more in a machine that has a larger airgap because of wider tolerance limits. As discussed in [17], manufacturing tolerance allows up to about 5 % eccentricity.

TABLE I. SURVEY OF UMP IN DIFFERENT MACHINES

Machine (star connected unless otherwise stated)	Method	Supply freq. [Hz]	Airgap g [mm]	Rotor Dia. D [m]	Axial length L [m]	Series turns N_{phase}	UMP [N]	Pole pairs p	Ecc. δ [p.u.]	Line voltage [V]	UMP coeff.	UMP factor	UMP-gap factor
10 pole blank rotor [15]	**Measured**	50	1.5	0.30	0.20	270	1450	5	0.4	415.0	0.88	1.14	3.41
10 pole blank rotor 5 parallel paths [15]	**Measured**	50	1.5	0.30	0.20	54	400	5	0.4	83.0	0.24	4.12	12.37
10 pole blank rotor 10 parallel paths [15]	**Measured**	50	1.5	0.30	0.20	27	80	5	0.4	41.5	0.05	20.61	61.83
10 pole cage rotor, Static Ecc, no load [15]	**Measured**	50	0.5	0.30	0.20	270	200	5	0.4	415.0	0.12	8.24	8.24
10 pole cage rotor, Dynamic Ecc, no load [7]	Simulated	50	0.5	0.30	0.20	270	600	5	0.4	242.5	1.07	0.94	0.94
10 pole cage rotor, Static or Dyn., locked rotor [7]	**Measured**	50	0.5	0.30	0.20	270	1400	5	0.4	207.8	3.39	0.30	0.30
4 pole synchronous machine, delta connected, (no load), Fig 1(a)	**Measured**	50	0.51	0.23	0.10	272	1125	2	0.4	259.8	1.39	0.72	0.73
4 pole synchronous machine, delta connected (load), Fig. 1(a)	**Measured**	50	0.51	0.23	0.10	272	350	2	0.3	83.1	5.63	0.18	0.18
4 pole cage induction, dynamic eccentircity, vibration test (no load) [7]	**Measured**	50	0.5	0.16	0.15	180	1100	2	0.45	300.0	1.25	0.80	0.80
6 pole cage induction motor (DC test - no rotor current), Fig. 1(b)	**Measured**	60	0.55	0.18	0.17	96	1458	3	0.73	140.0	1.03	0.97	1.07
4 pole rare earth surface magnet(no load) [25]	Simulated	200	1	0.07	0.05	63	270	2	0.5	172.6	0.25	3.99	7.98
4 pole rare earth consequent pole (no load) [25]	Simulated	200	1	0.07	0.05	63	524	2	0.5	172.6	0.49	2.06	4.11
12 pole fractional slot surface magnet (no load) [17]	Simulated	50	0.76	0.08	0.05	492	24	12	0.1	25.3	0.54	1.87	2.84
12 pole fractional slot surface (load) [17]	Simulated	50	0.76	0.08	0.05	492	35	12	0.1	25.3	0.78	1.28	1.95
12 pole fractional slot consequent rotor (no load)[17]	Simulated	50	0.76	0.08	0.05	492	47	12	0.1	25.5	1.03	0.97	1.47
12 pole fractional slot, consequent rotor (load) [17]	Simulated	50	0.76	0.08	0.05	492	90	12	0.1	25.5	1.98	0.51	0.77

Conclusions

This digest develops a UMP factor and UMP-gap factor which attempt to quantify the UMP to allow direct comparison of machines of different types and sizes. The UMPs from direct measurement that are reported here, and results from past literature, show that the factor appears to give a reasonable indicator. New UMP rigs are discussed that will allow direct measurement of the UMP which are flexible to the point of allowing both steady radial pulls and vibrations to be measured on individual bearings. This will allow rotor eccentricity which varies down the axial length to be studied and also skew effects. These will be reported in the full paper.

References

[1] D. G. Dorrell, "The sources and characteristics of unbalanced magnetic pull in cage induction motors with either static or dynamic eccentricity", Stockholm Power Tech, IEEE International Symposium on Electric Power Engineering, Stockholm, Sweden, 18-22 June 1995, Volume on Electrical Machines and Drives pp 229-234.

[2] P. Vijayraghavan and R. Krishnan, "Noise in electric machines: a review", IEEE Trans on Industry Applications, Vol. 35, No. 5, Sep/Oct 1999, pp 1007 – 1013.

[3] Z. Q. Zhu, D. Ishak, D. Howe, J. Chen, "Unbalanced Magnetic Forces in Permanent-Magnet Brushless Machines With Diametrically Asymmetric Phase Windings", IEEE Trans. Magn., vol. 43, no. 6, 2007, pp 1544 - 1554.

[4] J. Faiz, B. M. Ebrahimi and H. A. Toliyat, "Effect of Magnetic Saturation on Static and Mixed Eccentricity Fault Diagnosis in Induction Motor," IEEE Trans. on Magn. vol. 45, no. 8, Aug. 2009 pp 3137 - 3144.

[5] D. G. Dorrell, W. T. Thomson and S. Roach, "Analysis of airgap flux, current and vibration signals as a function of the combination of static and dynamic airgap eccentricity in 3-phase induction motors", IEEE Trans. on Industry Applications, Vol. 33, No.1, Jan. 1997, pp 24-34.

[6] R. Belmans, W. Heylen, A. Vandenput and W. Geysen, "Influence of rotor-bar stiffness on the critical speed of an induction motor with an aluminium squirrel cage," IEE Proc., vol. 131, pt. B, no. 5, Sept. 1984, pp 203 - 208.

[7] D. G. Dorrell, "Sources and Characteristics of Unbalanced Magnetic Pull in 3-Phase Cage Induction Motors with Axial-Varying Rotor Eccentricity", IEEE Trans. on Ind. Appl., vol 47, no. 1, Jan/Feb. 2011, pp 12-24.

[8] R. Perers, U. Lundin, and M. Leijon, "Saturation Effects on Unbalanced Magnetic Pull in a Hydroelectric Generator With an Eccentric Rotor," IEEE Trans. on Magn., vol. 34, no. 10, Oct. 2007, pp 3884 - 3890.

[9] L. Wang, R. Cheung, Z. Ma, J. Ruan, Y. Peng, "Finite-Element Analysis of Unbalanced Magnetic Pull in a Large Hydro-Generator Under Practical Operations," IEEE Trans. on Magn., vol. 44, no. 6, June 2008, pp 1558 - 1561.

[10] K. P. P. Pillai, A. S. Nair and G. R. Bindu, "Unbalanced Magnetic Pull in Train-Lighting Brushless Alternators With Static Eccentricity," IEEE Trans. on Veh. Tech., vol. 57, no. 1, Jan 2008, pp 120 - 126.

[11] J. T. Li, Z. J. Liu and L. H. A. Nay, "Effect of Radial Magnetic Forces in Permanent Magnet Motors With Rotor Eccentricity," IEEE Trans. on Magn., vol. 43, no. 6, June 2007, pp 2525 - 2527.

[12] I. Husain, A. Radun, and J. Nair, "Unbalanced Force Calculation in Switched-Reluctance Machines," IEEE Trans. on Magn., vol. 36, no. 1, Jan. 2000, pp 330 - 338.

[13] D. G. Dorrell, I. Chendurza and C. Cossar, "Effects of Rotor Eccentricity on Torque in Switched Reluctance Machines", IEEE Transactions on Magnetics, Volume 41, Issue 10, Oct. 2005, pp 3961 - 3963.

[14] D. G. Dorrell, "Experimental Behaviour of Unbalanced Magnetic Pull in 3-Phase Induction Motors with Eccentric Rotors and The Relationship with Tooth Saturation", IEEE Trans. Energy Conv., Vol. 14, No. 3, 1999, pp 304-309.

[15] D.G. Dorrell, A.C. Smith, "The calculation and measurement of unbalanced magnetic pull in cage induction motors with eccentric rotors. Part 2: Experimental investigation", 1996 Proc. IEE Elec Power Appl., Vol. 143, pp 202-210.

[16] D. G. Dorrell, "Calculation of unbalanced magnetic pull in small cage induction motors with skewed rotors and dynamic rotor eccentricity", IEEE Transactions on Energy Conversion, 1996, Vol 11, No3, pp 483-488.

[17] D. G. Dorrell, M. Popescu and D. Ionel, "Unbalanced Magnetic Pull due to Asymmetry and Low-Level Static Rotor Eccentricity in Fractional-Slot Brushless Permanent-Magnet Motors with Surface-Magnet and Consequent-Pole Rotors", IEEE Transactions on Magnetics, Vol 46, No. 7, pp 2675-2685, July 2010.

[18] I. P. Brown, D. M. Ionel and D. G. Dorrell, "Influence of Parallel Paths on Current Regulated Sine-Wave Interior Permanent Magnet Machines with Rotor Eccentricity," IEEE Trans. Ind. Appl., Vol. 48, Iss. 2, 2012, pp 642-652.

[19] A. Arkkio, M. Antila, K. Pokki, A. Simon and E. Lantto, "Electromagnetic force on a whirling cage rotor", Proc. IEE Electric Power Appl., Vol. 147, pp 353-360, 2000. A. Burakov and A. Arkkio, "Comparison of the Unbalanced Magnetic Pull Mitigation by the Parallel Paths in the Stator and Rotor Windings," IEEE Trans. on Magn., vol. 43, no. 12, Jan. 2007, pp 4083 - 4088.

[20] Y. Asano, A. Mizuguchi, M. Amada, A. Chiba, M. Ooshima, M. Takemoto, T. Fukao, O. Ichikawa and D. G. Dorrell, "Development of a Four-Axis Actively Controlled Consequent-Pole-Type Bearingless Motor", IEEE Transactions on Industry Applications, July/Aug 2009.

[21] H. M. Kelk, A. Eghbali and H. A. Toliyat, "Modeling and analysis of cage induction motors under rotor misalignment and air gap eccentricity", IEEE IAS Annual Meeting, Vol. 2, pp 1324 - 1328, 2005.

[22] S. Williamson and M. A. S. Abdel-Magied, "Unbalanced magnetic pull in induction motors with asymmetrical rotor cages", Proc. of 2nd Int. Conf on Electrical Machines - design and application, 1985, pp. 218-222.

[23] S. Williamson, M. A. Mueller, J. F. Eastham and L. H. Lim, "Transient unbalanced magnetic pull in change-pole induction motors", Proceedings of 4th IEE Electrical machines and drives conference, 1989, pp. 261-265.

[24] A.C. Smith, D.G. Dorrell, "The calculation and measurement of unbalanced magnetic pull in cage induction motors with eccentric rotors. Part 1: Analytical model", 1996 Proc. IEE Elec Power Appl., Vol. 143, No. 3, pp 193-201.

[25] D. G. Dorrell, M.-F. Hsieh and Y. Guo, "Unbalanced Magnet Pull in Large Brushless Rare-Earth Permanent Magnet Motors with Rotor Eccentricity", IEEE Transactions on Magnetics, Oct 2009.

[26] A. Chiba, T. Fukao, O. Ichikawa, M. Oshima, M. Takemoto, D. G. Dorrell, Magnetic Bearings and Bearingless Drives, Newnes, 2005.